Advanced Physics Laboratory

Franck-Hertz Experiment

Name: Nicolò De Masi, Manthan Chattopadhyay

Experiment Date: 28.06.2024

Abstract

Influenced by the Franck-Hertz experiment, this report investigates interaction of thermionic electrons with gaseous mercury and neon. Using electron tubes, we measured contact potential for two different heating voltages. The velocity distributions at room temperature and 60°C were derived by measuring current at the anode for varying retarding potentials. For mercury, we also determined the excitation energy of the $6^3P_1 \rightarrow 6^1S_0$ transition and analyzed the emission spectrum. Similar experiments were conducted for neon using a commercial Franck-Hertz tube.

Contents

1 Theoretical Background

James Franck and Gustav Hertz presented their paper 'On the collisions between electrons and molecules of mercury vapor and the ionization potential of the same' to the German Physical Society in 1914 [1]. Though not the intended purpose of its conception, the experiment validated the quantized nature of atomic energy levels, as proposed by Niels Bohr a year prior. It was shown that upon collision with mercury atoms, the fast electrons could lose only a *specific quantity* of their kinetic energy, while the slow electrons merely bounce off mercury atoms without losing significant kinetic energy.

1.1 Bohr Model: Proposal of Quantization

Even though Bohr's atomic model was an attempt to explain the observed line spectra of the elements, it served as a precursor to quantum theory. The following set of assumptions were made:

1. Balancing electrostatic Coulomb forces of attraction against the centrifugal effect and inter-electronic repulsion of classical orbital motion is necessary for dynamical equilibrium of stationary orbits.
2. These stationary states also satisfy the quantization condition where ratio of kinetic energy of the electron to its orbital frequency is an integral multiple of $\pi\hbar$.
3. Emission of energy only occurs when electrons perform a non-continuous (i.e. discrete) transition between two stationary orbits. The frequency of said emission is determined by $\Delta E/2\pi\hbar$, where ΔE is the energy difference of the two transition orbitals.

Total energy of electrons on a circular orbit of radius r and velocity v is

$$E = \frac{m_e v^2}{2} - \frac{Ze^2}{r} \tag{1}$$

Note that Z is the net positive nuclear charge. Since angular momentum $|\mathbf{L}| = |\mathbf{r} \times \mathbf{p}| = m_e v r$, which from Bohr's quantization assumption satisfies $L = n\hbar$, equation (1) becomes,

$$E_n = \frac{n^2\hbar^2}{2m_e r^2} - \frac{Ze^2}{r} \tag{2}$$

Minimizing $E \equiv E(r, n, Z)$ with respect to r,

$$E_n = -13.6\frac{Z^2}{n^2} \text{ eV} \tag{3}$$

and a quantized radius associated with each primary quantum number n,

$$r_n = \frac{n^2 a_0}{Z} \tag{4}$$

where $a_0 = 0.0529$ nm is the Bohr radius [2]. If a photon of energy $E = h\nu$ is absorbed/emitted, resulting in an electronic transition $n_i \to n_f$, equation (3) can be modified to

$$\nu = 13.6\frac{Z^2}{h}\left(\frac{1}{n_f^2} - \frac{1}{n_i^2}\right) \tag{5}$$

Despite being a violation of the uncertainty principle, and not being able to explain other quantum phenomenon such as fine and hyperfine structure observed in spectral lines, it provides a satisfactory framework for understanding electron transitions in hydrogen like atoms.

1.2 The Frank-Hertz Experiment

The objective of the experiment conducted by J. Franck and G. Hertz was to ascertain the velocity distribution of electrons both before and after their collisions with molecules of a diluted gas. The setup used in their experiment is shown below:

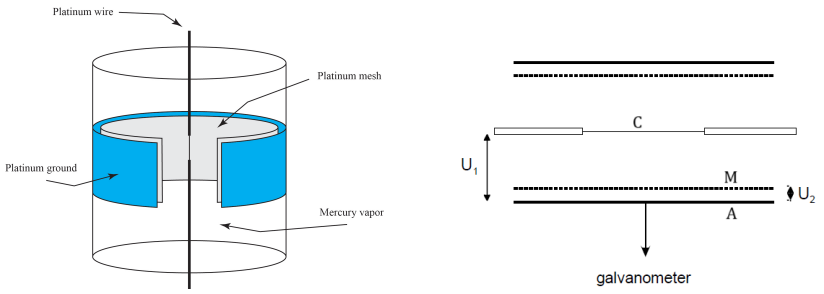

(a) (b)

Figure 1: (a) Original Franck-Hertz tube [3] and (b) cross-section with applied voltages [4]

The sealed glass tube contains few drops of mercury that produces controllable density of mercury vapour when the tube is heated. The central platinum wire (C) acts as a cathode as random heat motion causes thermionic emission of electrons from its surface. A mesh of fine platinum wires (M) is placed close to the anode (A) and usually has a diameter of about 4 cm. The current at the anode is measured with the help of a galvanometer. The mesh's voltage is positive relative to the cathode such that electrons are accelerated towards it. An acceleration voltage U_1 which can be adjusted is applied between C and M, with a constant retarding potential U_2 between M and A. Any measured current will be due to electrons that pass through the mesh and reach the anode. They kept U_2 as part of the parameter space, and measured the dependence of measured current at A, in dependence on U_1. The result became the well-known current-voltage dependency:

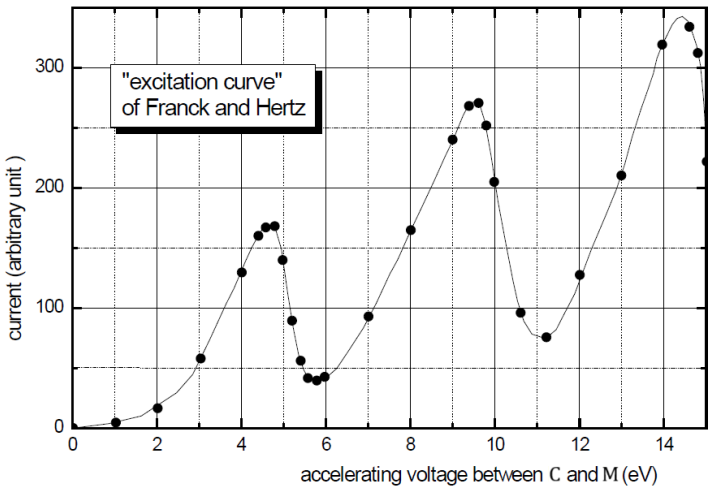

Figure 2: Current to counter electrode A as a function of accelerating voltage U_1 in mercury vapour [4]

Franck and Hertz interpreted Figure 4 as follows:

1. If $U_2 > U_1$, current will be zero as electrons will not possess sufficient acceleration to overcome the potential barrier beyond the mesh.

2. The current at the anode increases to a maxima till U_1 provides enough energy to the electrons to ionize the mercury atoms. The electrons close to the mesh undergo inelastic ionizing collision with mercury atoms. These and the electrons liberated from the ionization do not possess enough energy to pass the retarding potential barrier. This creates a valley where fewer electrons reach the anode.

3. Upon increasing U_1 further, the location where electrons experience inelastic collisions shifts closer to the internal platinum wire (C). The thermionic electrons now lose energy due to ionizing mercury atoms. The remaining energy of these electrons is the potential difference between the acceleration voltage and the ionization voltage. As they move towards the mesh, if this remaining energy (the potential difference) is greater than U_2, an increase in current is measured by the galvanometer. This increase is due to the ionization of mercury atoms, which creates more electrons, leading to a higher current than initially observed.

4. As U_1 reaches twice the ionization energy, electrons gain enough energy to undergo a second inelastic collision near the wiring network. This creates a re-iteration of observation (2), producing subsequent valleys and peaks.

5. The curve will have maximas of increasing height (more electrons produced overall due to higher order of ionization) in distances of integer multiples of the ionization voltage.

6. Assumed collision dynamics: Reflection occurs if an electron collides with KE lower than ionization energy. However, it experiences a loss in energy

related to electron affinity of the gas. If ionization is caused due to the collision, all KE is lost.

Note: It was later discovered that the measured energy actually corresponded to the excitation energy of the mercury atoms, not ionization energy. We will postpone this discussion to section 1.4.2

1.3 Properties of Electron Tubes

The cathode being the main source of current, needs to be heated to achieve efficient thermionic emission of electrons. A metallic conductor has an approximate electron density of 10^{22} cm^{-3}, with electrons performing a disordered movement due to thermal noise. In order to eject a large number of electrons off the surface of the metal, the cathode is heated to about 2000 K. The electrons with enough energy (or velocity) are able to leave the metal surface.

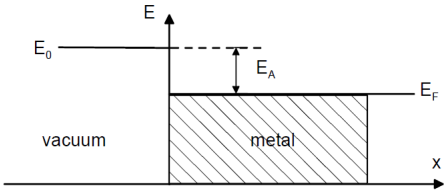

Figure 3: Potential relation at a metallic surface [4]

E_0 being the energy of electron at rest in vacuum nearby the surface, it holds that:

$$E_0 = E_F + E_A \tag{6}$$

where E_F is the Fermi energy and E_A the work function of the metal. Thus, E_A needs to be provided in order to remove an electron from the metal to a point in the vacuum immediately outside the surface. Assuming all ejected electrons contribute to the current, the total saturation current density i_s can be calculated as

$$i_s = \int_{E_A}^{\infty} ev(E)g(E)f(E)dE \tag{7}$$

where $v(E) = \sqrt{2E/m_e}$ with $g(E)$ and $f(E)$ being density of states and Fermi-Dirac distribution respectively. As a result one obtains the Richardson-Dushman law:

$$i_s = A_C T^2 \exp\left\{-\frac{E_A}{k_B T}\right\} \tag{8}$$

where the constant $A_C = 4\pi k_B^2 e/h^3$. Note that the saturation current has a strong dependence on cathode heating, i.e. the space charges formed within the tube are not taken into account. If we assign a negative voltage U_s on the anode, only the ejected electrons having an energy larger than eU_s are able to reach the anode. Taking their Maxwell velocity distribution into account, the running-in current conforms to the form

$$I = I_0 e^{\frac{eU}{k_B T}} \tag{9}$$

For $U = 0$, current tends to the saturation. For higher voltages, space charges occur. The transition from exponentially increasing current to saturation however,

does not occur at $U = 0$ but at a voltage corresponding to the contact potential E_K. Due to the difference in the work function of cathode an anode, we define

$$E_K = E_{\text{anode}} - E_{\text{cathode}} \tag{10}$$

This correction can be incorporated onto equation (9) as,

$$I = I_0 e^{\frac{eU - E_K}{k_B T}} \tag{11}$$

Thus, at $U = E_K/e$ the current is equal to the saturation current. For small heating currents, a straight line fit of the running in regime and saturation regime can provide a good approximation of the contact potential.

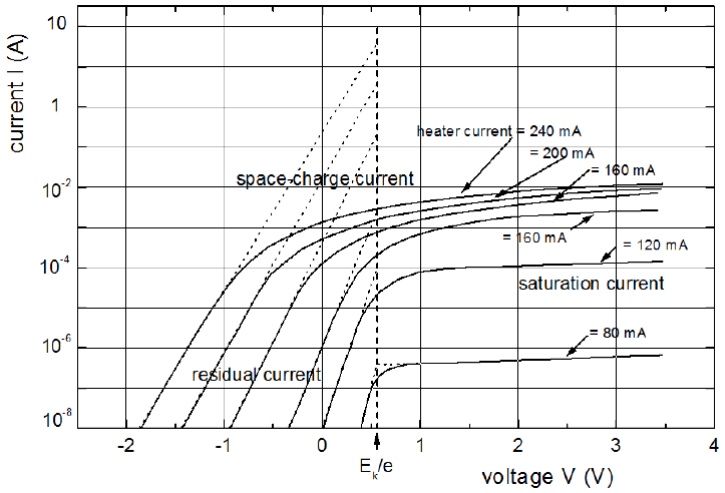

Figure 4: Characteristic I-U curve of an indirectly heated tube [4]

We observe that for high heating currents, the saturation regime sets in before the E_K/e point. The reason for this is the formation of space charge in the region between cathode and anode. This region is permanently filled by the same number of electrons. This negative charge limits the current through the tube, causing a premature saturation. From Barkausen 1962 [9], for $I < I_s$:

$$I = K\sqrt{U} \tag{12}$$

where K is a constant of the tube geometry.

1.4 Electron Tube with Mercury Vapor

We now discuss collision of the thermionic electrons with the mercury atoms in the tube. These collisions are classified by elastic and inelastic collisions. In the first case, electron energy is smaller than the lowest excitation energy of the mercury atoms, and the energy loss by the electron is negligible due to the substantial mass difference (200 a.m.u for Hg atom and 10^{-5} a.m.u for an electron). If the electron energy reaches the excitation energy threshold, inelastic collisions may occur, where the kinetic energy of the electron is transferred to

the mercury atom (which may be emitted as light). The scattering processes depend on our parameter space (i.e. particle energy, free path, tube temperature etc.).

1.4.1 Modelling Collisions & Opposing Field Method

We now consider the free path λ of the thermionic electrons in a mercury concentration of N. For simplification, we assume the Hg atoms to be at rest. One defines the scattering cross-section $\sigma = \pi(R_e + R_{Hg})^2$.

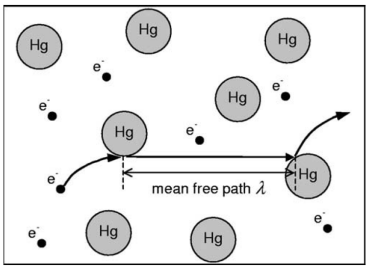

Figure 5: Schematic of the energy transfer from electrons to Hg atoms [10]

Upon covering a distance λ, the number of particles in a volume $V = \lambda\sigma$ is $NV = N\lambda\sigma$. If λ is large enough such that the electron collides with only one atom,

$$\lambda = \frac{1}{N\sigma} \tag{13}$$

The cloud of electron gas formed around the cathode (up till they are absorbed by the anode) can be modelled as an ideal gas by Maxwell's velocity distribution:

$$g(v)dv = \sqrt{\frac{2}{\pi}} \left(\frac{m}{k_B T}\right)^{3/2} v^2 \exp\left\{-\frac{mv^2}{2k_B T}\right\} dv \tag{14}$$

This distribution is famous for having an extended tail at high velocities as depicted in Figure 6:

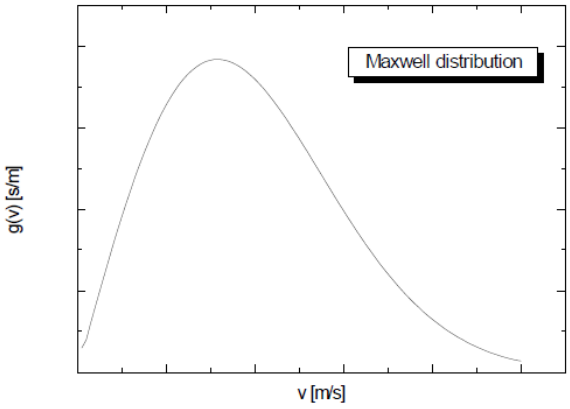

Figure 6: Maxwell distribution of an ideal gas at a fixed temperature [4]

For many processes such as impact ionization, determining the density of this high energy tail is necessary. The velocity distribution of the electrons at the anode post interactions can be experimentally determined with the opposing field method.

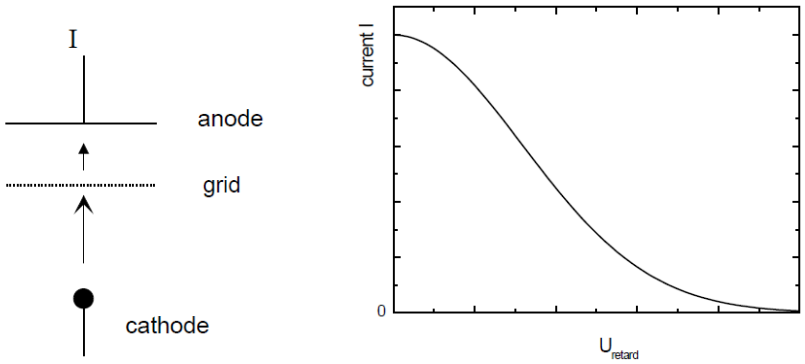

(a) (b)

Figure 7: (a) Opposing field method and (b) Current voltage dependence [4]

An accelerating voltage exists between the grid and cathode, while a retarding potential U_{retard} is introduced between grid and anode. The condition in order to reach the anode is now:

$$\frac{mv^2}{2} \geq eU_{\text{retard}} \tag{15}$$

Upon measuring the current at the anode against varying U_{retard}, one obtains a curve as shown in Figure 7 (b). Since current is proportional to number of electrons: within an interval $[U, U + dU]$, number of electrons $g(U)dU$ is proportional to $-dI$. Thus, it follows that:

$$g(U) \propto -\frac{dI}{dU} \tag{16}$$

We can obtain the energy distribution function by differentiating the I-U_{retard} curve.

1.4.2 Excitation Mechanism & Ionization of Mercury

Excitation mechanisms are based on the principle of incident photons (or in our case, accelerated electrons) transferring enough energy to the valence electrons in mercury atoms to effectively excite them, but not enough to eject them from the atom completely.

Mercury vapor atoms will normally be in their ground state, with the electronic configuration of two outermost valence electrons being $(6s)^2$ (two electrons in $n = 6$, with $l = 0 \equiv s$). The two electrons are bound by means of constant of motions designed by the quantum numbers **S** (total spin angular momentum), **L** (total orbital angular momentum, with $\mathbf{L} = 0, 1, 2... \equiv S, P, D...$) and **J** (total angular momentum).

These are usually indicated using spectroscopic notation, with the general form being: $(n)^{2\mathbf{S}+1}\mathbf{L_J}$.

The electrons in Hg ground state is thus denoted by 6^1S_0.

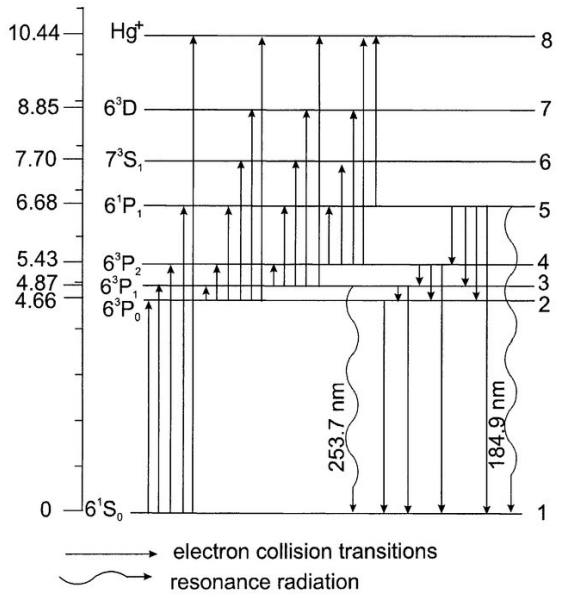

Figure 8: Energy levels of mercury [5]

When an electron in the ground state receives enough energy, it will transition to a higher state, with closer levels being more likely, as they require less energy. As shown in Fig. 8, the next level above the ground state is 6^3P_0, followed, in order, by 6^3P_1, 6^3P_2 and a higher singlet 6^1P_1 with anti-parallel spins. In a collision with an energetic electron with enough energy, atom could be raised into any of these excited states, however, in the Franck-Hertz experiment the main excitation observed is into 6^3P_1. This is because our measurements are dependent not on the transitions of electrons themselves to higher energy levels, but on their return to a steady state by the emission of a photon with energy (and thus wavelength) determined by the levels it transitions to and from.

This is normally a very rapid process, typically taking 10^{-8} s, which is instantaneous for the scope of our experiment.

However, photon relaxation transitions must satisfy conservation of total angular momentum **J**. The emitted photon carries away angular momentum with $\mathbf{J} = 1$. Thus, the total angular momentum quantum number of the atom must change by $\Delta J = \pm 1$ [6]. This entails that relaxation can occur from the 6^3P_1 and 6^1P_1 states, but not from even J states, which are metastable. These states undergo relaxation only through slower processes that typically take around 10^{-3} s.

If an electron in a mercury atom is excited to a metastable state during our experiment, it is stuck there for a millisecond and unable to absorb more energy. In the meantime, 6^3P_1 transitions would occur up to 10^5 times. The 6^1P_1 state is not usually observed because the lower state almost always absorbs energy from the electron beam. Once the electrons reach 4.87 eV, they are unable to acquire additional energy needed to excite the 6^1P_1 state, which requires 6.68 eV.

In the Franck-Hertz experiment, mercury's transition is dealt with as if it was uniquely defined by one single state (other than the ground state).

In reference to Fig. 8, we observe that if incident electrons on ground state electrons in mercury atoms possess more than 10.44 eV, enough energy will be transferred to eject the electron from the atom, effectively ionizing the atom into a positive ion. Subsequently, characteristic energies will be released as electrons relax to lower, more stable energy levels to fill the gap left by the ejected electron.

2 Experimental Setup

A commercial Franck-Hertz tube and a transmitting tetrode was used for this experiment.

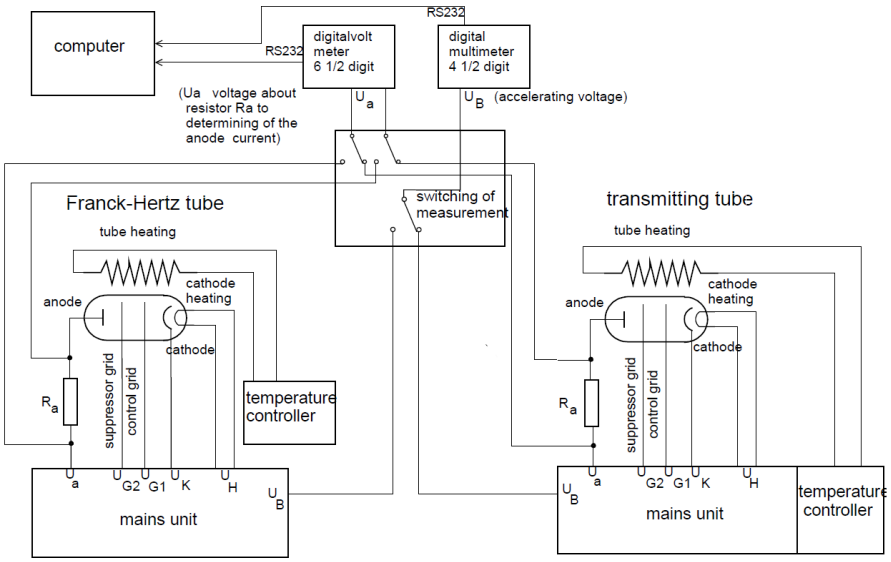

Figure 9: Schematic of the experimental setup [4]

The two tubes have independent temperature regulators and control devices. The necessary voltages are displayed digitally with the acceleration voltage being adjusted either via hand or automatically (at three different speeds). A test point switch and two digital voltmeters measure the anode current (voltage dissipation across R_a) and acceleration voltage. The computer receives a signal through serial interfaces, where the data is further analyzed. The temperature regulators lack a cooling option and act as a heater for a digitally pre-determined temperature. The transmitting tube has 3 operational modes that can be switched depending on the task at hand.

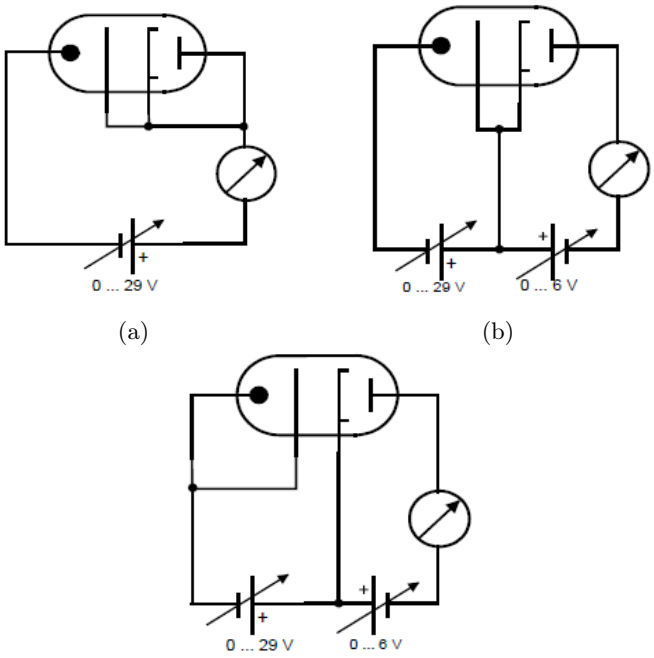

Figure 10: (a) Position 1 (b) Position 2 (c) Position 3 operating modes of transmitting tetrode [4]

Position 1 enables the automatic measurement of anode current and acceleration voltage. In mode 2, the two grids of the tube are connected in parallel. This aids us in the determination of velocity distribution as discussed prior in section 1.4.1. Mode 3 connects the grid in parallel to the cathode and will be used to determine ionization voltages for different reverse voltages.

3 Results & Discussion

3.1 Task 1: Tetrode Filled with Mercury

3.1.1 Contact Potential

As shown in equation (10), we now try to determine the contact potential. For small heating voltages, one derives a method for the determination of the voltage corresponding to the contact potential that involves the intersection of the running-in current "straight line" and of the saturation current "straight line" in the characteristic $I - U$ curve. This was done for two heating voltages of $U_h = 6$ V, 7 V. The accelerating voltage U_{acc} was varied automatically from 0 to 15 V. The measured voltage dissipation was converted into current knowing that the resistance was $R = 27\Omega$. The temperature, kept under monitoring thought the experiment, increased by around 4 °C.

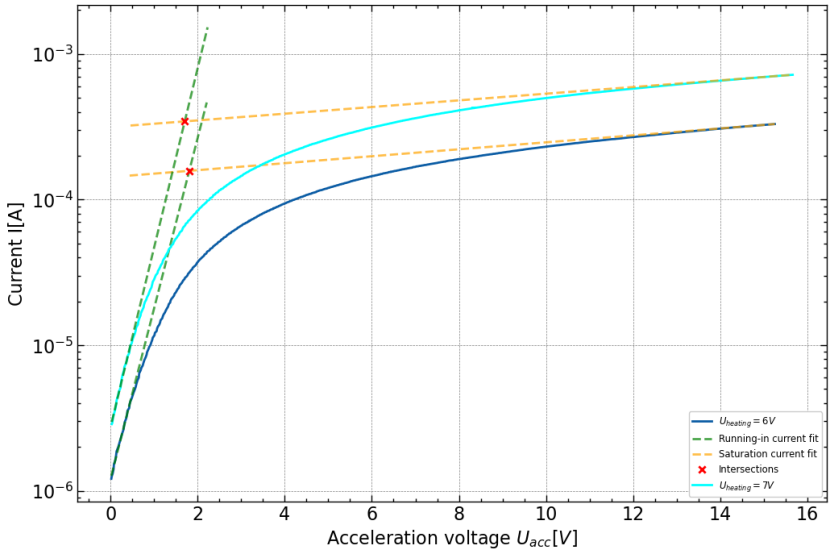

Figure 11: $I - U_a$ characteristic curves with intercepts

The contact potential E_k can be interpreted in units of eV as the energy difference caused by the difference in work function of the cathode and anode materials.

U_h[V]	U_k [V]	E_k [eV]
6	1.81 ± 0.07	1.81 ± 0.07
7	1.71 ± 0.07	1.71 ± 0.07

Table 1: Contact voltage and potential of Mercury for different heating voltages

When one considers the temperature fluctuations throughout the measurements and lack of accuracy with the method used to determine the contact voltage, a difference in E_k across different heating is expected. An average value of $E_k = 1.76 \pm 0.07$ eV is consistent with the finding of other similar experiments [11].

3.1.2 Velocity Distribution

In order to determine the velocity distribution of the thermionic electrons, we manually measure the voltage at the anode as a function of the counter voltage U_c. Since the internal resistance is again $R = 27\Omega$, we can find the current as $I = U_{\text{anode}}/R$.

This was performed for three different accelerating voltages $U_a = 6, 9, 12V$ at two different temperatures $T = 30, 60$ °C, while maintaining a heating voltage of $U_h = 7V$. Each set of measurement had a maximum temperature oscillation of ±3 °C.

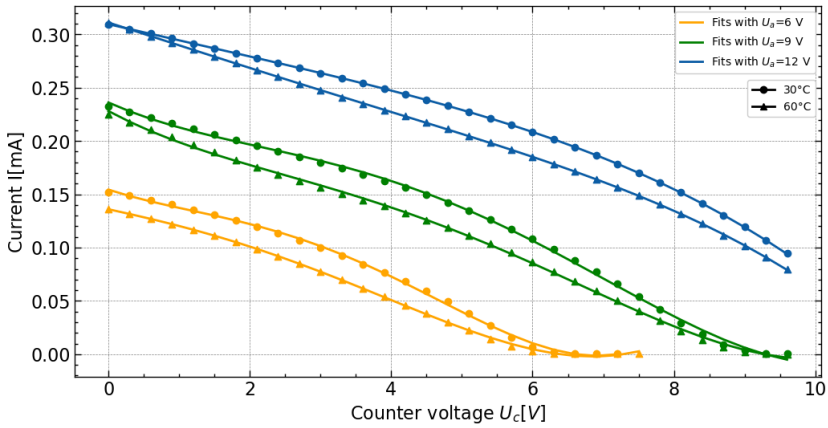

Figure 12: $I - U_c$ characteristic curves with polynomial fits

Each curve in figure 12 is interpolated as a fourth degree polynomial of the form:

$$I = a + bU_c + cU_c^2 + dU_c^3 + eU_c^4 \tag{17}$$

The parameters are the following:

	a	b	c	d	e
$I_{6,30}$	1.54×10^{-1}	-2.2×10^{-2}	7.2×10^{-3}	-2.6×10^{-3}	2.2×10^{-4}
$I_{9,30}$	2.36×10^{-1}	-3.0×10^{-2}	8.0×10^{-3}	-1.6×10^{-3}	9.0×10^{-5}
$I_{12,30}$	3.09×10^{-1}	-1.5×10^{-2}	1.2×10^{-4}	-2.3×10^{-5}	-7.1×10^{-6}
$I_{6,60}$	1.36×10^{-1}	-1.5×10^{-2}	-5.3×10^{-4}	-6.3×10^{-4}	8.6×10^{-5}
$I_{9,60}$	2.28×10^{-1}	-3.6×10^{-2}	7.7×10^{-3}	-1.4×10^{-3}	7.6×10^{-5}
$I_{12,60}$	3.11×10^{-1}	-2.1×10^{-2}	-2.3×10^{-4}	1.34×10^{-4}	-1.5×10^{-5}

Table 2: Fitted parameters for different sets of data.

We rewrite equation 17 in terms of the velocity using its relationship to the counter voltage 15:

$$I = a + \frac{bm}{2e}v^2 + \frac{cm^2}{4e^2}v^4 + \frac{dm^3}{8e^3}v^6 + \frac{em^4}{16e^4}v^8 \tag{18}$$

Equation (16) gives us the energy distribution function in terms of U_c. Setting $v^2 = k$, we find:

$$g(U_c) \propto -\frac{2e}{m}\frac{dI}{dk} \tag{19}$$

Differentiating equation 18 gives us the velocity distribution $g(v)$:

$$g(v) \propto -\left(b + \frac{cm}{e}v^2 + \frac{3dm^2}{4e^2}v^4 + \frac{em^3}{2e^3}v^6\right) \tag{20}$$

From which we obtain:

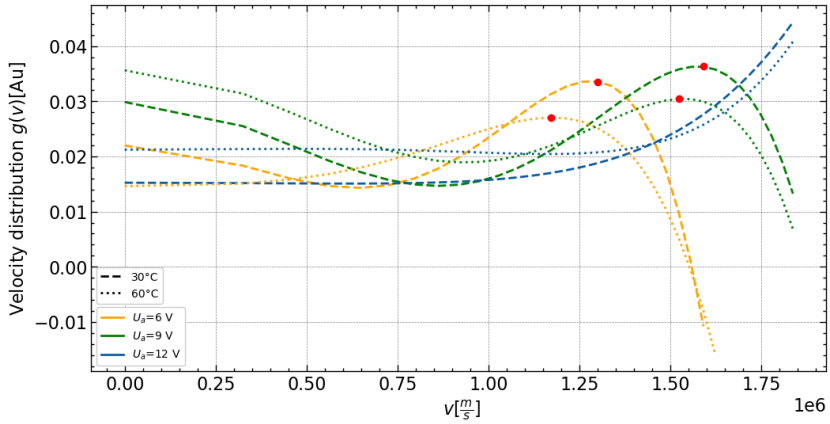

Figure 13: Velocity distribution

We can see that the most probable velocity consistently increases with accelerating voltage, while slightly decreases with respect to temperature (with the same U_a). For $U_a = 12$ V, our measurement range is too low to properly estimate the most probable velocity. For the remaining curves, the values are the following:

U_{acc} [V]	T [°C]	v [m/s]
6	30	1.171×10^6
6	60	1.299×10^6
9	30	1.524×10^6
9	60	1.591×10^6

Table 3: Most probable velocities from derived velocity distribution

3.1.3 Ionization Voltage

In this section our aim is to obtain an estimation for the ionization energy of mercury in the electron tube, with the use of the previously obtained contact potential. To that end we record characteristic curves by measuring the current in dependence on the acceleration voltage. We use three different reverse voltages $U_r = 1, 2, 3$ V, but maintain a constant heating voltage $U_h = 7$ V and temperature $T = 120 \pm 2$ °C. We obtain the following:

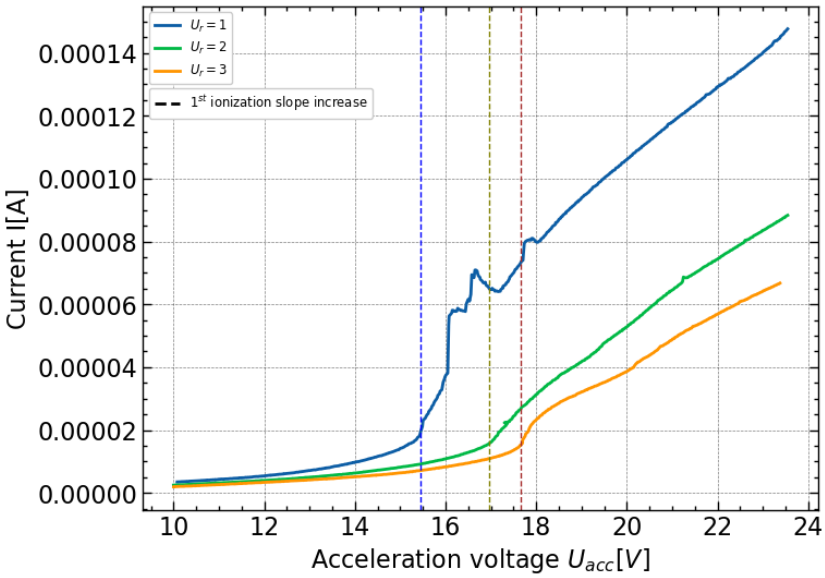

Figure 14: Ionization Voltages characteristic curves

The theoretical prediction is for the curves to show current plateaus alternated by instantaneous steep increases at critical acceleration voltages, where ionization theoretically take place, What we measure, however, does not entirely reflect our expectations, as there seems to be a substantial background constant current increase that worsen our results. Regardless of that, however, one can still (with substantially less certainty) estimate the point at which first ionization take place as the area where the slope of the curve increases.

The corresponding ionization voltages are then given by $U_i = U_{acc} - U_r - U_K$, where the contact potential is the one measured for $U_h = 7$ V i.e. $U_k = 1.71 \pm 0.07$ V. We thus have,

U_r	U_{acc} [V]	U_i [V]
1	15.45 ± 1	12.73 ± 1.07
2	16.96 ± 1	13.25 ± 1.07
3	17.67 ± 1	12.96 ± 1.07

Table 4: Ionization voltages of mercury

This yields an average ionization energy of $U_i = 12.98 \pm 0.07$ eV. Comparing with literature values of 10.44 eV, we have a deviation of around 24%. This is owed to both the methodology of determining E_K and the noise in the I-U$_acc$ curve.

3.2 Task 2: Investigations of the behaviour of Hg molecules in the gaseous phase

The aim of this task is to recreate the well known Franck-Hertz curve for mercury, from which we estimate the excitation energy of the resonance line (6^1S_0 to

6^3P_1). In the second part of the task, we verify our results by measuring the emission spectrum of a mercury lamp.

3.2.1 Measurements using a commercial Franck-Hertz Tube

The Franck-Hertz excitation curve is obtained by measuring the current at the anode against the accelerating voltage. The temperature was kept at 170 ± 0.1 °C for the entire measurement, the heating voltage at $U_h = 2.5$ V, and the counter voltage $U_c = 8$ V.

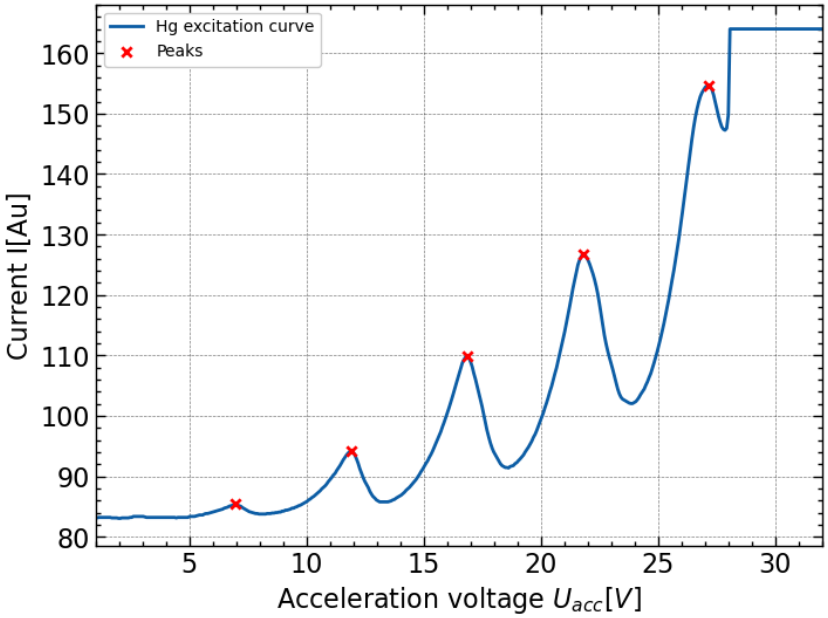

Figure 15: Franck–Hertz excitation curve for Mercury

Figure 15 clearly shows a series of valleys at approximately constant increments. From theory we know this behaviour to continue to potentials of at least 70 volts, but a lower range gives us enough data and a better definition of the first 5 peaks. A table follows:

peak index	U_{max} [V]	ΔU_{max} [V]
1	6.98	—
2	11.92	4.94
3	16.86	4.94
4	21.8	4.94
5	27.16	5.36

Table 5: Peak indexes with corresponding energies

Since the electrons' kinetic energies are again given by $E_k = Ue$, the excitation energy will correspond to the difference in voltage between successive peaks. An average over them gives (where the error corresponds to the standard error of the mean):

$$E_{ex} = (5.045 \pm 0.105)eV \tag{21}$$

This value is consistent with the theoretical value $E_{ex} = 4.89$ eV. Ideally, the distance between subsequent maximas would stay constant, but imprecision in the calibrations of the tools used and its limited resolution, as well as the unique amount of dataset taken for a single heating and counter voltage are limiting factors.

Additionally, using $E_{ex} = hc/\nu$, one predicts the wavelength of emitted photon due to the relaxation of the electron to the ground state as,

$$\lambda = (245.86 \pm 5.12)nm \tag{22}$$

3.2.2 Measurement of the Emission Spectrum of an Hg-Lamp

We now measure the wavelength of the emitted photons from a mercury lamp, disjoint from our Franck-Hertz setup. Due to the operating principle of the lamp, which employs vaporized mercury and then emits photons by ionizing (and exciting) it, a spectrum will show all the resonance lines which are of interests.

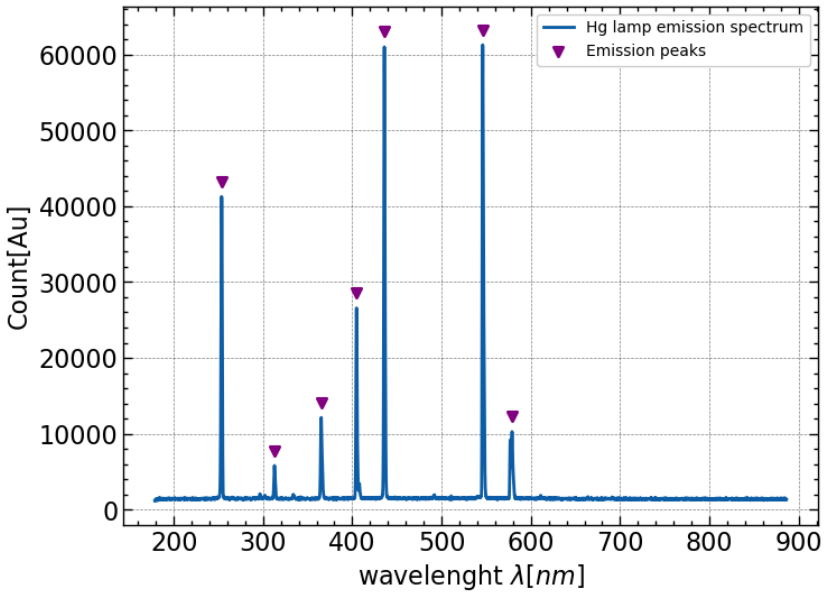

Figure 16: Spectrum of a mercury lamp

Fig. (16) shows distinctive peaks at different wavelengths, each of which can be associated with an energy (like in fig. (8)) and thus to the corresponding transition. We can assign a transition line to each peak, using the *NIST Atomic Spectra Database Lines Data* as reference [7].

Peak index	λ [nm]	E [eV]	Transition
1	253.62	4.889	$6^3P_1 \rightarrow 6^1S_0$
2	312.86	3.963	$6^3D_{1;2} \rightarrow 6^3P_1$
3	365.29	3.394	$6^3D_{1;2;3} \rightarrow 6^3P_2$
4	404.78	3.063	$6^3P_0 \rightarrow 7^3S_1$
5	435.95	2.844	$6^3P_1 \rightarrow 7^3S_1$
6	546.05	2.271	$6^3P_2 \rightarrow 7^3S_1$
7	578.98	2.141	$6^3D_1, 6^1D_2 \rightarrow 6^1P_1$

Table 6: Peak indexes with corresponding energies and transitions for mercury

Some transition lines have very similar theoretical energies, as such our peaks position will be the combination of the single events. Of special note is the first line corresponding to the $6^3P_1 \rightarrow 6^1S_0$ transition, since it was recognized in the first part of this task. The wavelength found with the Franck-Hertz Tube overestimated the lamp emission value by 3.06%.

3.3 Task 3: Investigations of the behaviour of Neon atoms in the gaseous phase

We now perform similar analysis for a neon tube. The working principle of this apparatus is similar to the mercury tube, enabling us to measure the excitation curve of Ne.

The advantage of using neon in the Frank-Hertz experiment is that the tube can be used at room temperature and thus not requiring the additional usage of heating; additionally, it provides visible evidences of energy levels [8]. The optimal conditions for our measurements where determined by the intensity of the orange glow between the cathode and the control grid. To understand the principle by which orange light is emitted, we need to discuss the electron configuration of Neon.

Neon is a significantly smaller element than Hg, and has 8 valence electrons $[(2s)^2(2p)^6]$ (the term symbol for the ground state is 2^1S_0).

Configuration	Term	J	Level (eV)
$2s^2 2p^6$	$2p^6\ {}^1S$	0	0.000 00
$2s^2 2p^5(^2P^o_{3/2})3s$	$3s[3/2]^o$	2	16.619 07
		1	16.670 83
$2s^2 2p^5(^2P^o_{1/2})3s$	$3s'[1/2]^o$	0	16.715 38
		1	16.848 05
$2s^2 2p^5(^2P^o_{3/2})3p$	3p[1/2]	1	18.38162
		0	18.711 38
$2s^2 2p^5(^2P^o_{3/2})3p$	3p[5/2]	3	18.55511
		2	18.575 84
$2s^2 2p^5(^2P^o_{3/2})3p$	3p[3/2]	1	18.61271
		2	18.636 79
$2s^2 2p^5(^2P^o_{1/2})3p$	3p'[3/2]	1	18.693 36
		2	18.704 07
$2s^2 2p^5(^2P^o_{1/2})3p$	3p'[1/2]	1	18.726 38
		0	18.965 96

Figure 17: Some of the energy levels of Neon [12]

The above table takes into consideration the excitation of a np^6 valence electron to a $np^5(n+1)p$ state, however, that is of course not the totality of all possible excitation levels. What one needs to consider is how close their energy levels are. This will contribute to the noise in our results, and prevent us from finding the exact energy for one excitation jump, as we will have multiple contributions.

The first levels above ground state present an excitation energy of about 16.62 eV, but have low probability of being excited. As such, a 18.7 eV interval is expected instead, representing the first level which consistently absorbs a ground electron. From there, the excited electrons first relax to the 16.6 eV levels (by the emission of orange photons, the ones we can actually observe), and only then relax further to the ground state (by emission of photons with wavelengths outside of the visible region of light). The observed excitation curve is the following:

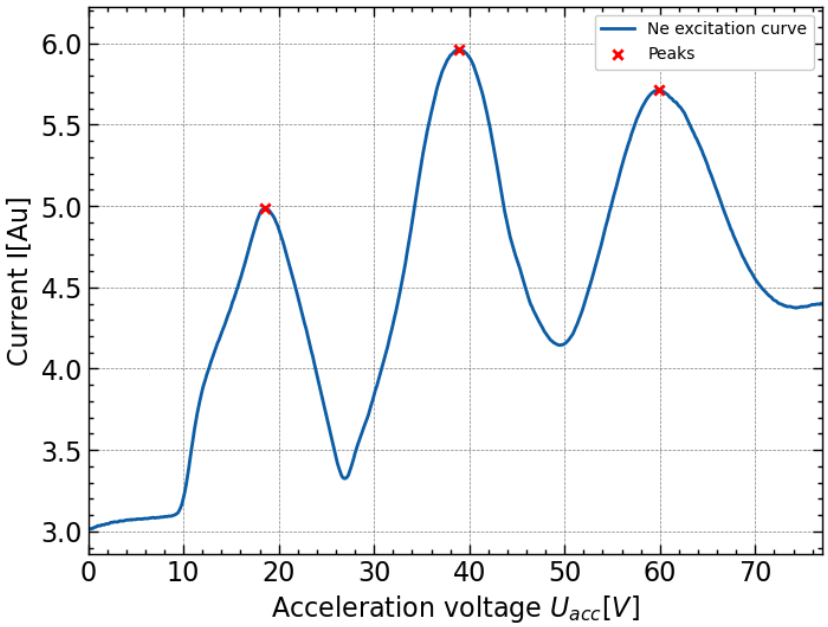

Figure 18: Franck–Hertz excitation curve for Neon

Following the same principle as for Mercury, voltage differences of successive peaks give an estimation for the excitation energy. We measure it to be:

$$E_{ex,Ne} = (20.645 \pm 0.356)eV \tag{23}$$

This is higher than the theoretical prediction, which can be owed to calibration and systematic errors associated with digitization of the signal, and the interference from multiple excitation levels as discussed before. Nevertheless, the corresponding wavelength is $\lambda_{ex,Ne} = (60.073 \pm 1.033)nm$.

4 Conclusion & Outlook

The setup in our laboratory successfully demonstrated the quantization of energy levels in mercury and neon atoms. For mercury, the measured contact potential of 1.76 ± 0.07 eV was consistent with similar studies. However, a deviation of 24% from literature values was observed for ionization energies, likely due to methodological limitations. The Franck-Hertz excitation curve yielded Hg excitation energy $E_{ex} = 5.045 \pm 0.105$, being very close to literature. Anomalies such as significant background current in mercury's ionization voltage measurements highlight areas for improvement. Lastly, neon presented a slight overshoot in excitation values. A cooling mechanism to reduce thermal noise is necessary for future studies.

References

[1] Franck J. Hertz G. (1914). *Über Zusammenstöße zwischen Elektronen und Molekülen des Quecksilberdampfes und die Ionisierungsspannung desselben.* Verhandlungen der Deutschen Physikalischen Gesellschaft. **16**: 457–467

[2] Chen G. Zhongai D. (2016). *Mathematical analysis of a Bohr atom model. Journal of Mathematical Physics.* **47**. 10.1063/1.2168396

[3] SKulls in the Stars (2023). Quantum Jumps: The Franck-Hertz experiment (1914). History of Science, Physics (URL: https://skullsinthestars.com/2023/05/20/quantum-jumps-the-franck-hertz-experiment-1914/)

[4] Riede V. (1999). *Franck-Hertz Experiment. Advanced Physics Laboratory.* University of Leipzig. Department of Physics and Geosciences

[5] Baeva, Margarita; Reiter, Detlev. (2003).*Monte Carlo Simulation of Radiation Trapping in Hg–Ar Fluorescent Discharge Lamps. Plasma Chemistry and Plasma Processing.* 23. 371-387. 10.1023/A:1022928320970.

[6] B. Zwiebach. (2013) *ADDITION OF ANGULAR MOMENTUM.* (URL: https://ocw.mit.edu/courses/8-05-quantum-physics-ii-fall-2013/f27e44d7b761cec0ef1d01734f0a23b8_MIT8_05F13_Chap_10.pdf)

[7] Kramida, A., Ralchenko, Yu., Reader, J., and NIST ASD Team (2023). NIST Atomic Spectra Database (ver. 5.11), [Online]. (URL:https://physics.nist.gov/asd [2024, June 24]. National Institute of Standards and Technology, Gaithersburg, MD. DOI: https://doi.org/10.18434/T4W30F

[8] Csele, Mark (2011). *"The Franck–Hertz Experiment". Fundamentals of Light Sources and Lasers.* John Wiley and Sons. pp. 31–36. ISBN 9780471675228.

[9] H. Barkausen: Lehrbuch der Elektronenröhren Bd.1, S.Hirtzel Verlag, Leipzig 1962

[10] Gerald Rapior, Klaus Sengstock, Valery Baev; New features of the Franck-Hertz experiment. Am. J. Phys. 1 May 2006; 74 (5): 423–428. https://doi.org/10.1119/1.2174033

[11] NEVA. Educational Products Corp. Franck-Hertz Experiment. (URL: https://web.mit.edu/8.13/8.13c/references-fall/franckhertz/old-tube-manuals-specifications.pdf)

[12] Kaur, Savinde; Srivastava, Rajesh ; Mceachran, Robert ; Stauffer, Allan. (1999). Excitation of the np5(n+1)p (J = 1, 2 and 3) states of the inert gases by spin-polarized electrons: integrated state multipoles and Stokes parameters. Journal of Physics B: Atomic, Molecular and Optical Physics. 32. 4331. 10.1088/0953-4075/32/17/316.